Acoust. Sci. & Tech. **28**, 3 (2007)

TRANSLATED PAPER

Direction separation in Doppler audio of ultrasound diagnosis equipment: Signal processing for Doppler audio dealiasing [1]

Tatsuro Baba*

Toshiba Medical Systems Corporation,
1385, Shimoishigami, Otawara, 324–8550 Japan

(*Received 22 May 2006, Accepted for publication 15 June 2006*)

Abstract: Medical Doppler ultrasound system has time varying spectrum display and Doppler audio stereo output based on blood flow. We examined the digital signal processing system of Doppler audio from a viewpoint of cost and size reduction. We newly developed the direction separation system of Doppler audio processing interlocking with spectrum Doppler image processing for aliasing. We made the target performance, developed three kinds of signal processing systems, and evaluated each system. Consequently, we could know that the complex IIR filter system was excellent in a response and low calculation load. We confirmed the Doppler audio signal processing for aliasing by simulation and could solve the problem caused by conventional system.

Keywords: Doppler ultrasound system, Direction separation, Aliasing, Doppler audio, Complex IIR band-pass filter, Baseline shift, Nyquist frequency

PACS number: 43.35.Yb [doi:10.1250/ast.28.202]

1. INTRODUCTION

A medical Doppler ultrasound system has a spectrum display that indicates the blood flow direction, whether the blood flows forward or away from a probe. It also has Doppler audio outputs. In particular, the latter is a special process peculiar to the Doppler ultrasound system and separates the blood flow direction and outputs from the left and right speakers.

In our previous studies [2,3], from the viewpoints of hardware downsizing and adjustment reduction, we examined the direction separation processing system of the Doppler ultrasound system. In this study, we developed a signal processing algorithm, which was described in our previous report, and introduced a new antialiasing processing system unique to the Doppler ultrasound system. We determined the target performance of a Doppler audio signal processing system, and compared three signal processing systems. Consequently, we clarified that a complex IIR (infinite impulse response) filter system has an excellent response and a low calculation load. Moreover, we confirmed by simulation that the Doppler audio direction separation process interlocks with the spectrum image process.

*e-mail: baba@us.nasu.toshiba.co.jp

2. ANTIALIASING DISPLAY AND CONVENTIONAL PROBLEM

The Doppler ultrasound system extracts the blood flow component used in the quadrature detection of the Doppler signal from the blood (mainly an erythrocyte), which moves inside a blood vessel, and removes a reflective signal from fixed things, such as a blood vessel wall organization, with a high-pass filter, and transforms the Doppler component into an image and sound.

The Doppler ultrasound system is shown in Fig. 1. The signal obtained after HPF processing is divided into two subsystems. Spectrum image processing generates a Doppler signal as a spectrum time change image corresponding to blood velocity, and Doppler audio processing outputs direction separation signals as stereo sound from the right and left speakers. Because the Doppler signal contains phase information, the signal includes both positive-side and negative-side frequency components. If sampling frequency is set to be f_s, the detection of a Doppler frequency component corresponding to the frequency range of $-f_s/2$ to $+f_s/2$ is possible. A spectrum image is shown in Fig. 2. The horizontal axis corresponds to time. The vertical axis corresponds to the speed derived from Doppler shift frequency, and luminosity corresponds to the spectrum intensity of each time. Since a spectrum image is a power spectrum generated by complex FFT processing, it

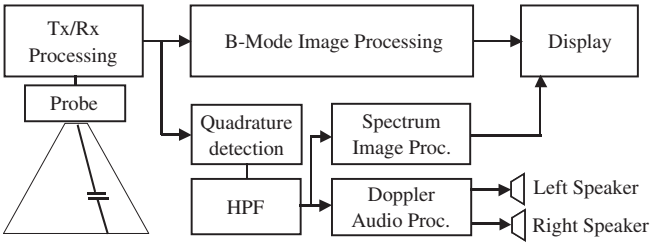

Fig. 1 Doppler ultrasound system.

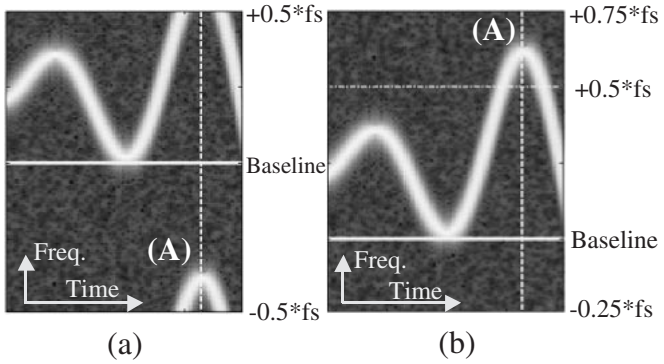

Fig. 2 Spectrum Doppler image. (a) Baseline shift = 0, (b) Baseline shift $= -0.25 * f_s$.

has the frequency range of $-f_s/2$ to $+f_s/2$ on the baseline (0 Hz) shown in Fig. 2(a). At the time (A) in Fig. 2, the frequency of the spectrum exceeds $+f_s/2$ and aliasing is induced. The Doppler ultrasound system has an antialiasing display function (BLS: baseline shift) that shifts a baseline to a negative side, as shown in Fig. 2(b), and expands a positive velocity range seemingly. Thus we can measure the peak velocity of blood flow easily.

The power spectrum at the zero baseline shift is shown in Fig. 3(a). The spectrum image at the $-0.25 * f_s$ baseline shift and the power spectrum corresponding to the time (A) in Fig. 2 are shown in Fig. 3(b). In the spectrum image, a baseline shift is easily realized by changing the frequency read-out operation of the spectrum after FFT processing. However, since there is no baseline shift function in the Doppler audio, a baseline shift is not realized in Doppler audio processing interlocking with spectrum imaging. For example, although a negative component is lost in the spectrum image shown in Fig. 3(b), since Doppler sound is still in the state shown in Fig. 3(a), it has a negative channel output and does not correspond to the Doppler image.

3. ANTIALIASING PROCESSING OF DOPPLER AUDIO

3.1. Target Performance

To solve the problem of the spectrum image and Doppler audio not working together, we examined the

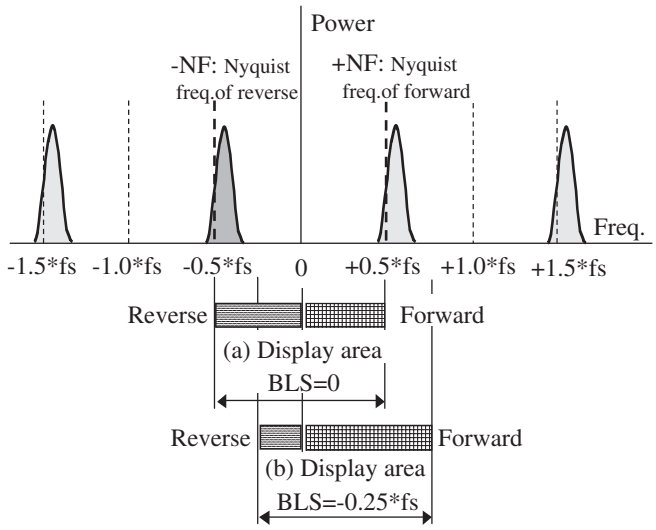

Fig. 3 Spectrum display area and baseline shift.

signal processing system of the Doppler audio to determine the possible type of baseline shift. The method of using mutual correlation with an RF signal before quadrature detection was reported as a method of detecting the movement of blood flow and clutter, in addition to spectrum Doppler signal processing [4,5]. On the other hand, since IQ signals after quadrature detection had merit at a small operation load in narrow-band processing, we examined a realization method based on the IQ signals. The Hilbert transform, complex FIR filter, phase shift, complex IIR filter, FFT/IFFT and modulation/demodulation systems also indicated that the direction separation system of the Doppler audio does not allow a baseline shift [2,3].

Among these systems, the Hilbert transform and phase shift systems enable direction separation by addition and subtraction between signals with a 180 degree phase difference. Since an input IQ signal has a 90 degree phase difference, these systems give more phase difference of 90 degrees between channels with a filter. Since the phase difference of an IQ signal stops being 90 degrees when sampling frequency is doubled as a countermeasure, in the Hilbert transform and phase shift systems, which make the phase difference between channels a simple 90 degrees, direction separation is difficult. Moreover, the complex FIR filter system involves the same preprocessing step as that in the complex IIR filter system, and antialias processing becomes possible. However, since the length of a FIR coefficient sequence doubles, the operation load increases. On the other hand, the FFT/IFFT system can reduce the operation load by diverting the FFT output of spectrum Doppler imaging processing (equivalent to spectrum imaging processing in Fig. 1). When the FFT output is diverted, the returning antialias processing can be performed only by inverse FFT and shift addition. The

Table 1 Target specification of Doppler audio processing.

Item	Target
1. Time delay	bellow 20 ms ($f_s = 4$ kHz)
2. Direction split	above 30 dB
3. Frequency characterization	$\pm 1/128$–$\pm 127/128 * f_s$ flat as possible
4. Frequency resolution	$f_s/100$
5. Baseline shift range	$-f_r/2$–$+f_s/2$

Table 2 Frequency shift and bandwidth table of baseline shift.

Baseline shift	−0.5	−0.25	0	0.25	0.5
FB: band width of forward	4/8	3/8	2/8	1/8	0
FBC: center freq. of forward	4/16	3/16	2/16	1/16	0
RB: band width of reverse	0	1/8	2/8	3/8	4/8
RBC: center freq. of reverse	0	−1/16	−2/16	−3/16	−4/16

Notes: Baseline shift, *FB*, *FBC*, *RB* and *RBC* are normalized by f_s.

modulation/demodulation and complex IIR filter systems mainly involve the multiplication of modulation/demodulation and IIR filter processing. Thus, their calculation processing is easy, and the increase in calculation load by antialiasing processing is small.

As mentioned above, from the viewpoints of calculation load reduction and antialias processing feasibility, we chose and examined the following three systems: the modulation/demodulation, FFT/IFFT, and complex IIR systems. When evaluating these systems, we showed the same target performance required as that of the Doppler ultrasound system in Table 1.

Delay time: A user usually sets up the Doppler range gate on a tomogram, moves it, and performs blood flow diagnosis with the Doppler ultrasound system. In searching for a small blood vessel, the Doppler audio is effective, because its response is faster than that of the spectrum image. This is because a tomogram set with the Doppler audio delays the outputs of about 20 ms, compared with the spectrum image that has a typical delay of about 40 ms. The time delay of tomogram processing (equivalent to B mode image processing in Fig. 1) is a few cycle of one frame (13.3–16.7 ms). In the Doppler signal processing system, it has a total processing delay of 10 ms by quadrature detection and HPF processing, except for the Doppler processing part (equivalent to Doppler audio processing in Fig. 1). Therefore, to make the tomogram and audio agree, a time delay of 3.3–6.7 ms is required at the Doppler signal processing part. However, because the direction separation process, which is the main factor of the Doppler signal processing part delay, requires a number of series samplings for processing, a target time delay is theoretically difficult to achieve. Therefore, the target time delay was set to be 20 ms or smaller, so that the target delay time required for the direction separation process to store the Doppler audio is about one frame cycle at maximum in a tomogram.

Capability of direction separation: It has been reported that human direction distinction requires a right-and-left signal difference of 15–20 dB or lager [6]. In an actual Doppler ultrasound system, considering that the Doppler signal has a broad band, that the angle between the right and left speakers is small, and that blood flow movement changes with time, a larger signal difference is required. The target performance of direction separation was set to be 30 dB or higher at observation frequency.

Frequency characteristic: A signal processing frequency range is the range f_s from negative-side Nyquist frequency to positive-side Nyquist frequency (equivalent to −NF–+NF in Fig. 3), where f_s is input IQ signal sampling frequency. To add antialiasing processing to this, we made the frequency characteristic flat in the region of $\pm 1/128$–$127/128 * f_s$ range.

Frequency resolution: Since spectrum image signal processing involves 256-point FFT, an acceptable frequency (blood velocity) resolution is obtained. However, when the frequency resolution of the Doppler audio is unacceptable, similar to that of a small-pitch Doppler image, we set the target resolution to be $f_s/100$. The frequency range is determined from sample frequency. However, the frequency resolution is proportional to the reciprocal of observation time. For example, in FFT, it is equivalent to the main robe width of the sampling function [7] determined from observation time width and the window function.

Baseline shift range: The baseline shift range is considered to be $-0.5 * f_s$–$+0.5 * f_s$ to enable range expansion on the positive and negative sides to twice the Nyquist frequency range. The ranges of both sides correspond to the baseline shift shown in Table 2. *FB* and *RB* indicate the bandwidths on the positive (forward) and negative (reverse) sides, whereas *FBC* and *RBC*, the center frequencies on the same sides, respectively. These are normalized using f_s. Although five stages were used from the baseline shift range of −0.5 to +0.5 in this example, a small setup is possible with the actual Doppler ultrasound system.

Others: The calculation load is also an important factor for evaluating performance, although it is not used in evaluating the target performance shown in Table 1. The calculation load is so advantageous that a low cost, a reduced size, and a low power consumption are obtained, although it is dependent on the hardware architecture, such as DSP, ASIC, and FPGA.

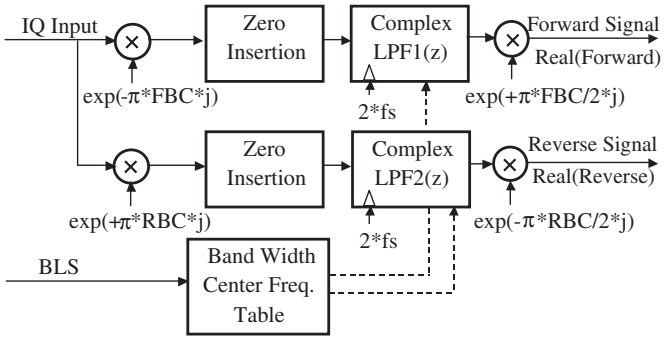

Fig. 4 Block diagram of modulation/demodulation system.

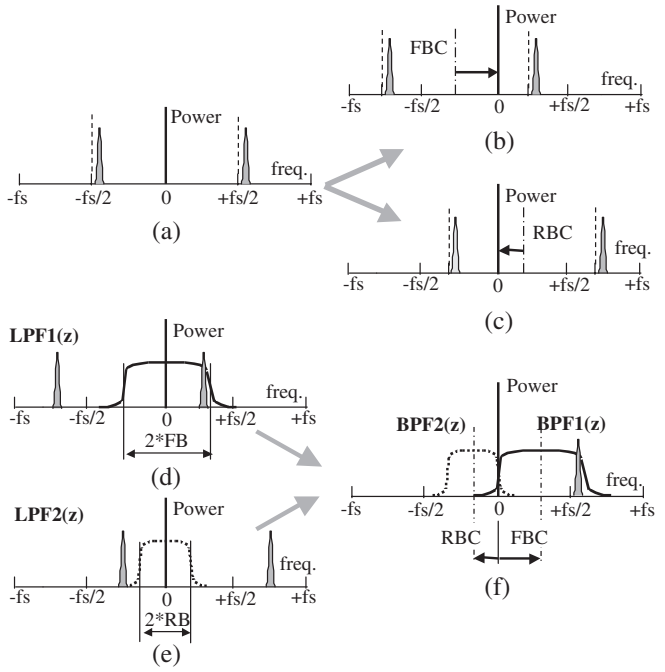

Fig. 5 Frequency design of modulation/demodulation system. (a) Spectrum of IQ input, (b) Spectrum of forward modulation, (c) Spectrum of reverse modulation, (d) Spectrum of complex LPF1, (e) Spectrum of complex LPF2, (f) Spectrum of demodulation.

3.2. Modulation/Demodulation System

The block diagram of the modulation/demodulation system [8] is shown in Fig. 4. The IQ signal is modulated with two sets of quadrature modulators. Thereby, the frequency of the signal induces a $+FBC$ shift on the positive side and a $-RCB$ shift on the negative side. Next, Nyquist frequency is doubled by zero insertion [9,10], and signals are demodulated by applying band limitations on the positive and negative sides. The input signal (equivalent to (A) in Fig. 2) with the aliasing spectrum in Fig. 5(a) is modulated, and the spectra indicating the $+FBC$, and $-RCB$ shifts of the frequency of the signal are shown in Figs. 5(b) and 5(c), respectively. A positive-side component and a negative-side component are extracted by carrying out a baseline shift and applying a band limitation using the bandwidths of $\pm FB$ and $\pm RB$ in the passage regions of $LPF1(z)$ and $LPF2(z)$. The spectra of the $LPF1(z)$ and $LPF2(z)$ outputs are shown in Figs. 5(d) and 5(e). Since sampling frequency has doubled after an LPF output, the direction separations on the positive and negative sides that shift the frequencies of $-FBC/2$ and $+RCB/2$ by demodulation, and are denoted by $BPF1(z)$ and $BPF2(z)$ in Fig. 5(f) are realizable. Although the spectrum in Fig. 5 (equivalent to the aliasing (A) in Fig. 2) is outputted to the negative side for the Nyquist frequency $f_s/2$, it can extract the positive-side component beyond the Nyquist frequency in Fig. 5(f). The operation was changed and performed in the calculation example shown in Table 3. For response improvement, we did not use a FIR filter for LPF but the 8th IIR filter with an equivalent performance.

3.3. FFT/IFFT System

The block diagram of the FFT/IFFT system is shown in Fig. 6. Two sets of filters corresponding to the baseline shift separate the IQ signal after FFT processing. These filters are realized by applying $WF(\omega)$ and $WR(\omega)$ with the characteristics of FB, RB, FBC, and RBC shown in Table 2. Next, the separated spectra are returned to the time domain signals by inverse FFT. Since the frequency range expands on the basis of the baseline shift, we perform twice-point inverse FFT. Further shift addition in time waveform after inverse FFT is carried out, and a continuous output is obtained. The power spectrum of the IQ signal after FFT is shown in Fig. 7(a). When the baseline shift is terminated, the spectrum in the figure (equivalent to the aliasing (A) in Fig. 2) is observed on the negative side. However, by operating the read-out address of FFT, the positive display range is expanded and observed on the positive side. Similarly, by carrying out inverse FFT processing with $WF(\omega)$ and $WR(\omega)$ with a frequency twice that of sampling $(2 * f_s)$, the frequency range of the Doppler audio is expanded, and the positive-side component in Fig. 7(b) and the negative-side component in Fig. 7(c) are obtained. In the calculation example

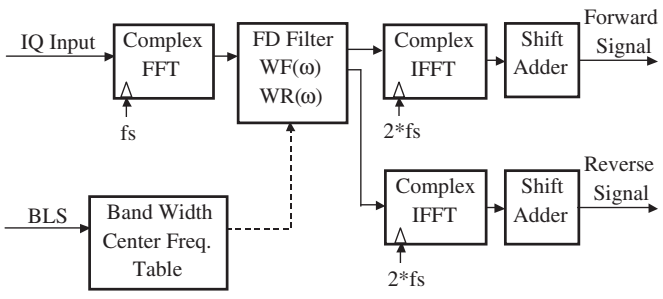

Fig. 6 Block diagram of FFT/IFFT system.

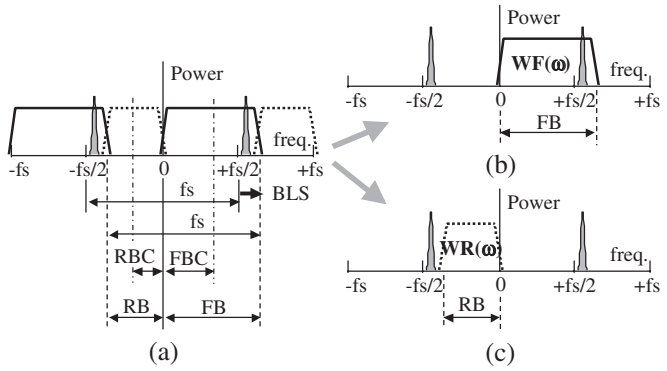

Fig. 7 Frequency design of FFT/IFFT system. (a) Spectrum of IQ input, (b) IFFT forward component extracted by $WF(\omega)$, (c) IFFT reverse component extracted by $WR(\omega)$.

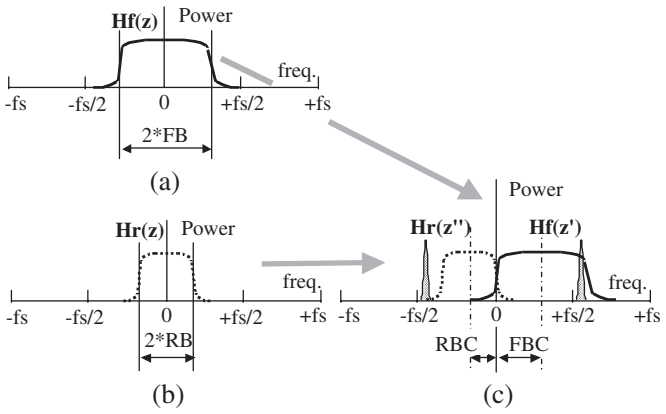

Fig. 9 Frequency design of complex IIR filter system. (a) Spectrum of LPF $Hf(z)$, (b) Spectrum of LPF $Hr(z)$, (c) Spectra of complex BPF $Hf(z')$ and $Hr(z'')$.

shown in Table 3, we perform 128-point FFT and 256-point inverse FFT. Moreover, we perform the shift addition of 32 time series data to which the Hamming window is applied after inverse FFT.

3.4. Complex IIR Filter System

The signal processing block diagram of the complex IIR filter system is shown in Fig. 8. Zero insertion is carried out with a pretreatment, and Nyquist frequency is increased. Next, two complex band-pass filters separate both components directly. The frequency characteristics of the transfer functions $Hf(z)$ and $Hr(z)$ with the bandwidths of FB and RB (one side bandwidth) for LPF are shown in Figs. 9(a) and 9(b). On the basis of the Fourier transform shift theory [11], the frequency shifts (FBC and RBC) are applied to z operators, and a transfer function of LPF changes to the positive-side and a negative-side band-pass filters [12,13]. Operator z is transformed to $z' = z * \exp(-j * FBC)$ and $z'' = z * \exp(-j * RBC)$.

The frequency characteristics of the complex band-pass filters $Hf(z')$ and $Hr(z'')$ enable the $+FBC$ and $-RBC$ frequency shifts are shown in Fig. 9(c) [14,15]. In the calculation example shown in Table 3, we use the 8th Butterworth filter by considering the response of direction separation.

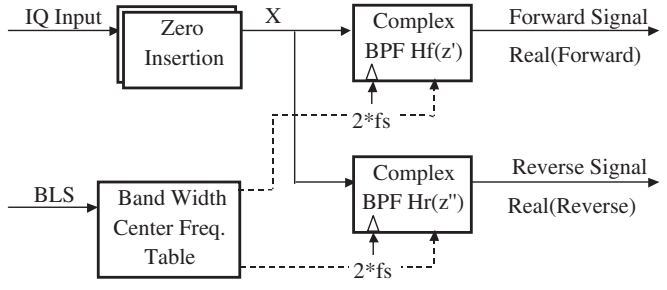

Fig. 8 Block diagram of complex IIR filter system.

3.5. Performance Comparison

To satisfy the target performances of frequency resolution and frequency characteristics shown in Table 1, we set up parameters for all the systems, such as the order of the filters and the FFT number. We use the 8th Butterworth filter with cutoff $0.495 * FB * f_s$ and $0.495 * RB * f_s$ for the LPFs of the modulation/demodulation and complex IIR filter systems. We perform 128-point FFT and 256-point inverse FFT involved in the FFT/IFFT system, and we apply rectangular weight to $WF(\omega)$ and $WR(\omega)$. First, the delay times theoretically determined from the above-mentioned parameters and calculation loads are shown in Tables 3 and 4, respectively. Since the signal processing input is sampled using f_s, delay time increases with a decrease in f_s. Table 3 shows the delay time calculation result for a typical $f_s = 4\,\mathrm{kHz}$ diagnostic operation. Moreover, we simply estimate the delay from the calculation load itself considered to be zero by sampling, and the estimated values are not affected by the transient response. Since the operation load depends strongly on the hardware architecture that performs signal processing, we evaluate the frequency of multiplication/addition for 1 s (single-accuracy floating point). The complex multiplication load is set to be 4 times and the complex addition load is set to be twice the real operation. Moreover, the processing that requires memory transmission, such as zero insertion processing and buffer

Table 3 Time delay of Doppler audio processing.

Method	Estimation	Delay [ms]
Mod./demod.	order/f_s (*1)	2 (order = 8)
FFT/IFFT	$0.75 * N/f_s$ (*2)	24 ($N = 128$)
Complex IIR	order/f_s (*1)	2 (order = 8)

Delay is estimated at $f_s = 4\,\mathrm{kHz}$. (*1) not including transient response. (*2) IFFT shift addition pitch is $N/4$.

Table 4 Calculation load of Doppler audio processing.

Method	Calculation component	Estimation equation	Load [MFLOPS]
Mod./ demod.	Cadd: order $*$ 8 $*$ f_s Cmul: (order $*$ 8 + 6) $*$ f_s Ovh: 20%	$f_s * (48 * \text{order} + 24) * 1.2$	1.96 (order = 8)
FFT/IFFT	Cadd: $N * r1 + 4 * N * r2$ Cmul: $N * r1/2 + 2 * N * r2$ Rmul: $2N * 6$ Ovh: 20%	$(2f_s * 4/N) * N$ $* (12 + 6 * r1 + 12 * r2) * 1.2$	5.76 ($N = 128$) ($r1 = 7$, $r2 = 8$)
Complex IIR	Cadd: order $*$ 8 $*$ f_s Cmul: order $*$ 8 $*$ f_s Ovh: 20%	$f_s * (48 * \text{order}) * 1.2$	1.84 (order = 8)

Radd: real addition, Rmul: real multiplication, Ovh: over head, Cadd: complex addition, Cmul: complex multiplication, IFFT shift addition pitch is $N/4$. Calculation volume is estimated at $f_s = 4$ kHz.

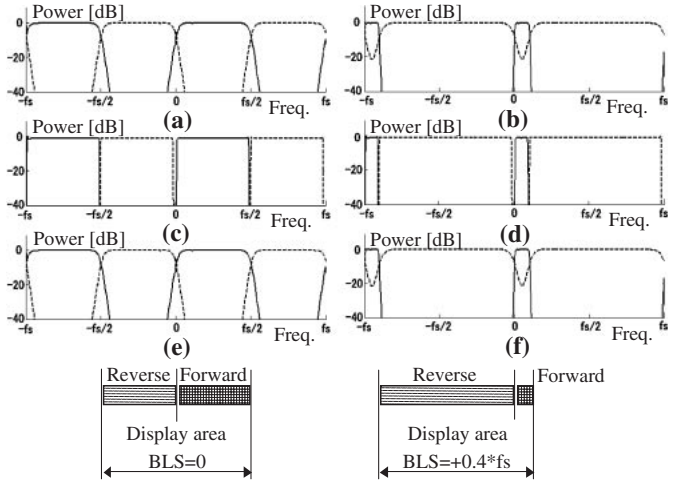

Fig. 10 Frequency characterization of Doppler audio output. (a) Modulation/demodulation system: $BLS = 0$, (b) Modulation/demodulation system: $BLS = +0.4 * f_s$, (c) FFT/IFFT system: $BLS = 0$, (d) FFT/IFFT system: $BLS = +0.4 * f_s$, (e) Complex IIR filter system: $BLS = 0$, (f) Complex IIR filter system: $BLS = +0.4 * f_s$.

processing, is included in overhead processing. The operation load of overhead processing is estimated as 20% of total multiplication/addition operation load.

The calculation element for every signal processing system, calculation-load estimated formula and operation load per second ($f_s = 4$ kHz) are shown in Table 4. The estimated results in Tables 3 and 4 show that the complex IIR filter and modulation/demodulation systems are fulfilling the delay time performance goal. Regarding the calculation load, the complex IIR filter system is the smallest, the modulation/demodulation system is slightly larger, and the FFT/IFFT system is the largest, but still small compared with previously reported values. Next, we perform a simulation to check whether we can meet the frequency feature of the performance goal in Table 1. We sweep the frequency of the input IQ signal and measure the powers of the positive-side and negative-side outputs.

We evaluate simultaneously the frequency features and direction separation performance at this time. The frequency features of the direction separation output according to the three signal processing systems are shown in Fig. 10. A solid line denotes the positive-side component, and a dashed line, the negative-side component. The horizontal axis indicates the frequency range from $-f_s$ to $+f_s$. Moreover, the spectrum image display range corresponding to the frequency range is shown in the bottom rail. The output feature of the Doppler audio at the zero baseline shift is shown in Figs. 10(a), 10(c) and 10(e), and that of $+0.4 * f_s$ baseline shift is shown in Figs. 10(b), 10(d) and 10(f). From these results, we confirm that the frequency feature in each signal processing system of the Doppler audio corresponds to the baseline shift of the spectrum image. Here, we consider that owing to the effect of the shift addition in the Hamming window of the FFT/IFFT system, the component near DC in Figs. 10(c) and 10(d) is missing. Since this missing part has a value lower than the typical setting value of cutoff frequency for the high-pass filter (equivalent to HPF in Fig. 1) of the preceding process, we do not encounter any problem. Moreover, we observe that the separation degrees of the positive-side component in Figs. 10(b) and 10(f) are insufficient. We consider that the cutoff features (the 8th Butterworth filter is used in the simulation) of the modulation/demodulation and complex IIR filter systems can be improved by making them steep. However, in the case of using an IIR filter, we should expand the internal bit length (dynamic range), because the increased load is expected to be affected by quantizing noise. For example, although Figs. 10(e) and 10(f) are calculated using the

single floating point (24-bit mantissa) in the simulation, by increasing cutoff frequency or filter order, mantissa bit length (accuracy) may be insufficient and the calculation load or hardware scale may increase. Although we use the Butterworth filter this time, we can choose the Chebysev filter and acquire a steep cutoff feature. On the other hand, the frequency feature and direction separation performance near cutoff frequency deteriorate with a ripple and rapid phase change. From now on, we are going to continue examining these trade-offs.

From the above results, we observe that in choosing the response and calculation load, the complex IIR filter system is the most effective. On the other hand, the FFT/IFFT system is the most effective in choosing the frequency feature, although the response is poor. Since the response is more important than the frequency feature clinically, and the target performance in Table 1 is fulfilled mostly, we consider the complex IIR filter system to be the best device for the direction separation of the Doppler audio system.

4. IMPLEMENTATION OF COMPLEX IIR FILTER SYSTEM

4.1. Signal Processing Simulation

We examine the possibility of using the complex IIR filter system in signal processing simulation. The input signal is conceived to be for the actual venous blood model. The model consists of a noise component (white noise), a blood vessel wall component (clutter: low frequency high power), and a blood flow component. The powers and frequencies of these components are shown in Table 5. The input and output waveforms and power spectra of the processing blocks in the complex IIR filter system are shown in Fig. 11. The amplitude of the left-hand-side waveform is normalized by clutter amplitude to be 2. Moreover, 256-point FFT with a Hanning window is applied to the calculation of the right-hand-side power spectrum. Figures 11(a) and 11(c) show the input and output waveforms of zero insertion processing, respectively. A solid line denotes the I component, and a dashed line, the Q component. Figures 11(e) and 11(g) show the Doppler audio outputs of both directions at the zero baseline shift. A solid line denotes the real component, and a dashed line, the imaginary component. Figures 11(i) and 11(k) show the Doppler audio outputs of both directions at the $+0.4 * f_s$ baseline shift. A solid line denotes the real component, and a dashed line, the imaginary component. Figures 11(b), 11(d), 11(f), 11(h), 11(i) and 11(l) show power spectra corresponding to the waveforms in the time domain. The aliasing spectra of blood flow and clutter are observed in Fig. 11(d) for a zero insertion processing output. Moreover, the approximately -20 dB DC component is observed at the center of the spectra. This DC component, which is not removed using the Hanning window, does not affect the latter complex band-pass filter processing. From the positive-side output waveform at the zero baseline shift shown in Fig. 11(e), we confirm that the blood flow component of $+0.24 * f_s$ frequency is separated on the positive side. Moreover, in the power spectrum shown in Fig. 11(f) in addition to the blood flow component, we observe that the clutter component ($-0.08 * f_s$) remains on the negative-side under the effect of the filter element. In the negative-side output waveform at the zero baseline shift in Fig. 11(g), the separation of the

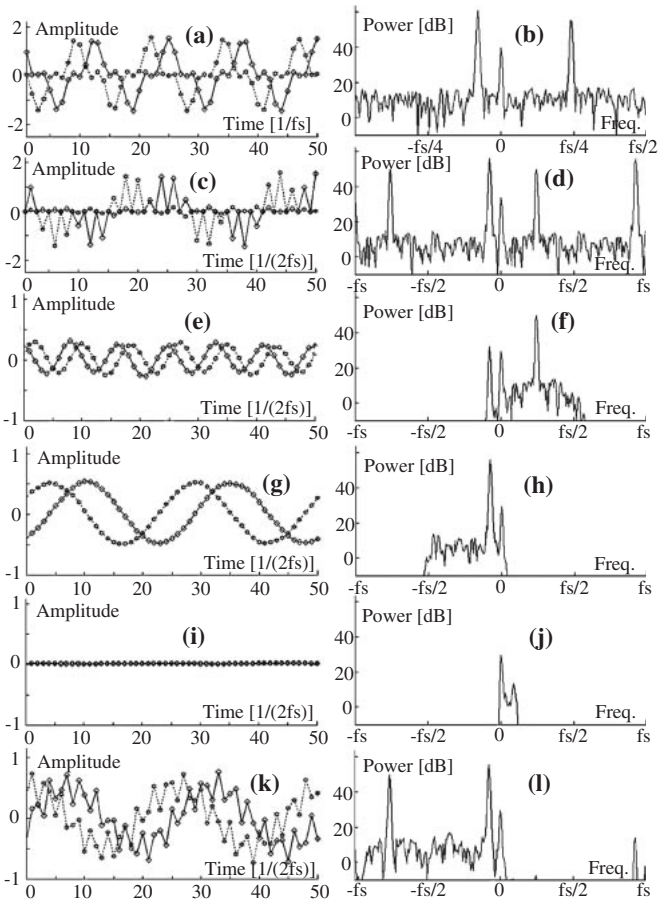

Fig. 11 Simulation waveform and spectrum of complex IIR filter system. (a) IQ input signal, (b) Power spectrum of (a), (c) After zero insertion waveform, (d) Power spectrum of (c), (e) Forward output ($BLS = 0$), (f) Power spectrum of (e), (g) Reverse output ($BLS = 0$), (h) Power spectrum of (g), (i) Forward output ($BLS = +0.4 * f_s$), (j) Power spectrum of (i), (k) Reverse output ($BLS = +0.4 * f_s$), (l) Power spectrum of (k).

Table 5 Components of simulation input model.

Components	Blood	Noise	Clutter
Power	-6 dB	-20 dB	0 dB
Frequency	$0.24 * f_s$	(white noise)	$-0.08 * f_s$

clutter component ($-0.08 * f_s$) is observed on the negative-side. Moreover, in the power spectrum in Fig. 11(h), a clutter component and a DC component are detected. When the baseline shift is $+0.4 * f_s$, the spectrum image and Doppler audio must generate a negative region larger than a positive region. The positive-side output waveform after the baseline shift in Fig. 11(i) shows the disappearance of the clutter component ($+0.24 * f_s$). Moreover, we confirm the absence of the blood flow component in the power spectrum shown in Fig. 11(j). We also confirm that a novel blood flow component ($-0.76 * f_s$), which is an alias component ($+0.24 * f_s$), is outputted into the negative-side output waveform after the baseline shift in Fig. 11(k), except for the clutter component ($-0.08 * f_s$). Moreover, in the power spectrum in Fig. 11(l), we confirm that the blood flow and clutter components are separated on the negative side.

4.2. Implementation

On the basis of the Doppler IQ signal of the carotid artery collected with the actual Doppler ultrasound system, an example of antialiasing signal processing of the Doppler audio is shown in Fig. 12. We use a string phantom (Mark 4 Doppler Phantom: JJ&A Instrument Company) and the ultrasonic diagnosis equipment (SSA-770A: Toshiba Medical Systems Corporation) for generating and collecting the Doppler signal. We use PLT-604AT (6.0 MHz linear probe) at a pulse repetition frequency (PRF) of 4 kHz equivalent to f_s. We collect the IQ data in the pulse wave Doppler (PWD) mode. Moreover, we set cutoff frequency at an HPF of 200 Hz for clutter removal. The output waveforms of both sides of the Doppler audio and spectrum image obtained from the IQ data are shown in Fig. 12. In this figure, in the vicinity of 0.9 s, the baseline shift is switched into $-0.4 * f_s$ from 0. At the zero baseline shift, we observe aliasing in the spectrum image shown in Fig. 12(a) and a negative-side output in Fig. 12(c). However, we confirm that the positive-side display range of the spectrum image expands after a baseline shift and is interlocked with the Doppler audio. Although it is not observed in Fig. 12, the characteristic of the band-pass filter changes immediately after a baseline shift. We will continue to examine the transient response of the Doppler audio under this effect and to consider implementation technologies, such as muting.

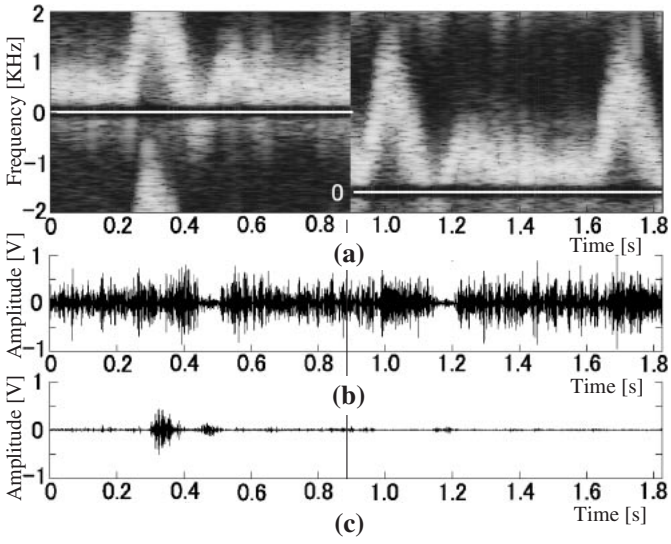

Fig. 12 Doppler spectrum display and audio output waveform. (a) Spectrum image, (b) Forward output, (c) Reverse output.

5. CONCLUSION

We developed the direction separation system of a Doppler audio interlocked with the antialiasing processing of a spectrum image using a complex IIR band-pass filter system.

First, we defined the target performance of Doppler audio processing and selected three signal processing systems. We developed processing algorithms and compared their performances. Consequently, we confirmed that the complex IIR band-pass filter system has an excellent response and a low calculation load.

Next, we performed functional and performance analyses by simulation with the data collected using a Doppler signal model and a phantom.

Conventionally, although in the antialiasing process unique to a Doppler ultrasound system, the image and audio did not correspond, since it was applied only to a spectrum image, we could solve this problem by signal processing.

REFERENCES

[1] English translation of the same article in *J. Acoust. Soc. Jpn. (J)*, **62**, 153–160 (2006).
[2] T. Baba, "The investigation of the audio direction separation in the Doppler ultrasound system Part 1: The comparison of the digital signal processing algorithm," *Proc. AI Acoust. Soc. Jpn.*, pp. 29–33 (2004).
[3] T. Baba, "The investigation of the direction split technique of the Doppler ultrasound: Comparison of six kinds of Doppler audio processing," *J. Soc. Signal Process. Appl. Technol. Jpn.*, **8**(2), pp. 14–20 (2005).
[4] S. I. Rabben, S. Bjaerum, V. Sorhus and H. Torp, "Ultrasound-based vessel wall tracking: an autocorrelation technique with RF center frequency estimation," *Ultrasound Med. Biol.*, **28**, 507–517 (2002).
[5] J. A. Jensen, "A new estimator for vector velocity estimation," *IEEE Trans. Ultrason. Ferroelectr. Ferq. Control*, **48**, 886–894 (2001).
[6] J. Blauert, *Spatial Hearing*, Revised Edition (The MIT Press, Cambridge, Mass., 1997), pp. 155–164.
[7] T. Araki, *Illustration: The Communication System Theory and Reality* (Kogaku Tosho Co., Inc., Tokyo, 1985), pp. 78–83.
[8] J. Koo, S. D. Otterson and Siemens Medical Systems Inc.,

"Method and system for Doppler ultrasound audio dealiasing," *United States Patent*, US5676148, Oct. 14 (1997).

[9] H. Takaie and S. Tsujii, *Multirate Signal Processing* (Shokodo Co., Ltd., Tokyo, 1995), pp. 28–39.

[10] K. Maeda, A. Sano, H. Takaie and S. Hara, *Wavelet Transform and Its Application* (Asakura Publishing Co., Ltd., Tokyo, 2001), pp. 55–59.

[11] R. N. Bracewell, *The Fourier Transform and Its Aplications* (McGraw-Hill Companies Inc., Boston, 2000), pp. 111–113.

[12] T. Baba, Y. Miyajima and Toshiba Corp., "Ultrasonic diagnosis equipment," *Open Patent Official Report*, Provisional Publication No. 10-99332, Apr. 21 (1998).

[13] T. Baba and Toshiba Corp., "Ultrasonic diagnostic equipment and the Doppler signal processing method," *Open Patent Official Report*, Provisional Publication of a Patent 2002-325767, Nov. 12 (2002).

[14] T. Baba, "Investigation on separation of ultrasonic Doppler signals: signal processing of Doppler aliasing," *Proc. AI Acoust. Soc. Jpn.*, pp. 3–4 (2004).

[15] T. Baba, "Investigation of the audio direction separation in Doppler ultrasound system: Signal processing of Doppler audio for aliasing," *J. Acoust. Soc. Jpn.* (*J*), **62**, 153–160 (2006).